Journal of Design Against Fatigue
https://minerva-aset.com/JDAF
MINERVA ASET ISSN 2976-940X

Rotating Bending Fatigue Durability of ferritic nitrocarburized Wrought 304 Stainless Steel: A Comparative Study of Surface-Treated vs. Untreated Specimen

Alireza Behvar [a], Onome Scott-Emuakpor [b], Bradley Crannell [c], Kevin James [c], Meysam Haghshenas [a, 1]

a Department of Mechanical, Industrial, and Manufacturing Engineering (MIME), the University of Toledo, OH 43606, USA
b Hyphen Innovations, Dayton, OH 45431, USA
c Turbocam International, Dover, NH 03820, USA

P A P E R I N F O

Paper history:
Received 10 September 2024
Received in revised form 22 October 2024
Accepted 25 October 2024

Keywords:
Rotating bending fatigue; stainless steel 304; surface treatment; machine learning.

A B S T R A C T

The rotating bending fatigue test, which is a common durability test for industrial components, was employed in this study to examine the impact of the surface treatment procedure on the material's performance under room temperature. The studied material in this research is wrought stainless steel (SS) 304 alloy that has undergone a specialized surface treatment (ferritic nitrocarburizing) to enhance the fatigue properties of this unique material. The fatigue endurance of untreated materials was 405 MPa (65% of untreated specimen's yield strength) on 5 million runout cycles, while the surface-treated samples exhibited 545 MPa (85% of treated specimen's yield strength), a significantly greater value compared to the untreated ones (even up to 10 million runout cycles). The experimental results demonstrated that the surface-treated samples exhibited no signs of cracking. Instead, all failures were attributed to plastic bending, particularly at higher stress levels. Furthermore, the samples displayed a limited range of stress levels, spanning from endurance to plastic bending conditions. This finding suggests that the hypothesis of an increase in strength in the surface layer is more pronounced than in the material interior. It also indicates that the surface layer material was not cracked under the maximum stress level, while the layer beneath it experienced plastic deformation. A comparison has been made between the Basquin equation and a statistical machine learning model (for a limited amount of data) to incorporate the impact of surface treatment on predicting fatigue lifetime, and the random forest regressor model would be able to predict the lifetime with the accuracy of R^2= 87% which was much higher than the classical model.

https://doi.org/10.62676/jdaf.2024.2.2.10

1. INTRODUCTION

Austenitic stainless steels (SS), such as SS304, are extensively utilized in several industries, including aerospace [1, 2] and chemical processing [3, 4], due to their exceptional corrosion resistance, formability, and mechanical qualities. Nevertheless, the fatigue characteristics of these materials, particularly when subjected to rotating bending circumstances, are currently being investigated due to the intricate factors introduced by surface conditions and treatment procedures. Surface treatments are frequently used to improve the fatigue life of a material by altering surface characteristics like hardness, residual stress, and roughness [5, 6]. These modifications play a critical role in delaying the formation and spread of cracks. Given the significant impact of surface conditions on crack initiation during fatigue tests [7, 8], particularly in rotating bending fatigue (RBF) tests [6, 9], studying the surface effect and implementing surface improvement treatments can be crucial in extending the lifespan of materials. The impact of surface treatment on the fatigue properties of SS304 has consistently been a captivating subject for the industry. Several surface treatment techniques,

1 Corresponding Author meysam.haghshenas@utoledo.edu

Cite this article as: Alireza Behvar, Onome Scott-Emuakpor, Bradley Crannell, Kevin James, Meysam Haghshenas, Rotating Bending Fatigue Durability of ferritic nitrocarburized Wrought 304 Stainless Steel: A Comparative Study of Surface-Treated vs. Untreated Specimen, ***Journal of Design Against Fatigue,*** Vol. 2, No. 2, (2024), 1-12, https://doi.org/10.62676/jdaf.2024.2.2.10

Copyright: © 2024 by the author(s). Published by Minerva ASET, Devon, UK. This is an open access article distributed under the terms and conditions of the Creative Commons Attribution (CC BY) License. (https://creativecommons.org/licenses/by/4.0/).

such as shot peening [10], surface hardening [11], and nitriding [12], have been studied to enhance the SS304 fatigue resistance. These treatments usually create compressive residual stresses on the surface [13-15], which oppose the tensile stresses that occur during repeated loading, thus enhancing the durability against fatigue. Shot peening has been proven to enhance the fatigue limit by creating a layer of compressive stress that obstructs crack formation on the surface [16, 17]. Similarly, the processes of nitriding and carburizing increase the hardness of the surface and decrease its roughness (in some cases increase), hence leading to enhanced fatigue performance.[18 ,12]

Yang et al. [10] conducted a study to examine the impact of shot peening on the fatigue characteristics of SS304. They demonstrated that shot peening led to an enhancement in both fatigue strength and fatigue limit. This improvement can be attributed to the distribution of residual compression stress on the surface after the treatment, which effectively prevents the opening of crack mouths during cyclic loading [19]. Similar findings were reported by Chung et al. [15]. Wiriyasaroj et al. [20] demonstrated that the boronized surface layer enhances fatigue resistance but may decrease the lifespan under high stress levels. All the surface treatments listed here will alter the properties of the surface layer while the internal layers may stay unaffected. The discrepancy between the surface layer's elevated yield strength and the interior's lower yield strength can result in plastic deformation at high stress levels [21]. The surface layer remains elastic, while the interior endures plastic deformation [22]. This phenomenon is a result of the mechanical property gradient that is introduced by surface treatments, such as shot peening or carburizing [23]. These treatments generate compressive residual stresses at the surface, which balance the tensile stresses within the core. Consequently, the material may undergo non-uniform deformation during cyclic loading, which may result in premature fatigue failure or unanticipated mechanical responses. It is essential to comprehend the interaction between fatigue behavior and surface treatment-induced property gradients to accurately predict the performance and durability of treated components in high-stress applications. Given all the mentioned phenomena, it is necessary to minimize the influence of the inner layers on fatigue attributes to have a more accurate knowledge of the effects of surface treatment. The RBF test, because of its ability to apply high stress on the surface and dully reverse stress amplitude, is the optimal choice for a detailed investigation of surface attributes [24, 25]. Consequently, the following question arises: If surface treatment improves the mechanical properties of the surface layer and thereby enhances fatigue endurance, what role does the interior layer play? Considering that mechanical properties vary from the interior to the surface, what is the maximum stress level that can be sustained for a given lifetime?

The present study aims to examine the impact of surface layer treatment on the enhancement of the S-N curve and the impact of plastic deformation in the interior layers while the surface layer is still in the elastic domain to address this question. The present study examines the impact of a proprietary salt bath ferritic nitrocarburizing (FNC) surface treatment (developed by Turbocam International) on the fatigue characteristics of wrought SS304 subjected to RBF test. The treatment is intended to enhance the surface properties of the material, consequently increasing its resistance to the beginning and spread of fatigue cracks. The fatigue performance of the treated specimens is compared to that of untreated specimens to evaluate the effectiveness of the treatment. This work provides a thorough examination of the fatigue characteristics of SS304 in both treated and untreated states, emphasizing the correlation between surface treatment and fatigue endurance. The results are anticipated to offer useful insights into the mechanisms via which surface treatments improve fatigue resistance, providing practical implications for the design and production of components that are resistant to fatigue.

2. EXPERIMENTAL PROCEDURE

The chemical composition of the SS304 material used in this investigation, as shown in Table 1, was supplied by the Turbocam International company. The CNC lathe machine was used to turn both test series specimens following ISO 1143 circular dog-bone fatigue samples as Fig. 1(a). The other set underwent a specific surface treatment procedure (salt bath FNC) that was developed by Turbocam International for their components. To ascertain the fatigue test stress levels, the F3L laboratory at the University of Toledo conducted a tensile test on both specimens using an MTS machine system based on the ASTM E8 standard.

Table 1: Chemical composition of the studied wrought SS304

C%	Cr%	Ni%	Mn%	Si%	Mo%	Cu%
0.016	18.28	8.09	1.88	0.54	0.58	0.58
Co%	**N%**	**P%**	**S%**	**Co%**	**N%**	**P%**
0.154	0.080	0.030	0.026	0.154	0.080	0.030

Based on the tensile test results, the stress levels for untreated specimens were selected as 65% to 82% of the yield strength, while for treated specimens, they ranged from 85% to 95%, as determined by their respective tensile properties. Typically, two tests were conducted for each stress level, except in cases where runout samples were used for step testing due to a limited number of specimens. Fatigue tests were performed using a rotating bending fatigue machine (Fig. 1(b)) at ambient temperature. Tests with stress levels greater than 80% were conducted at a frequency of 500 RPM, while those below 80% were conducted at 1000 RPM. The reduction in frequency at higher stress levels was necessary to mitigate self-heating, which caused sample temperatures to exceed 100°C. To prevent thermal effects, the frequency was lowered, and the sample temperatures were monitored with a pyrometer, ensuring they remained below 60°C.

Following the fatigue test, the fractured surfaces were examined using a scanning electron microscope (SEM). Only the untreated specimens exhibited fracture, as the treated specimens did not fracture (plastically deformed). The fractured surfaces were sectioned as shown in Fig. 2 and analyzed for fractography to identify crack initiation sites and propagation areas, providing crucial data for further modeling.

In developing the lifetime prediction model, fractography images were initially utilized to create a model based on fracture mechanics theories. However, due to low accuracy, machine learning (ML) techniques were later employed to analyze statistical data and develop a more reliable model based on the recorded features.

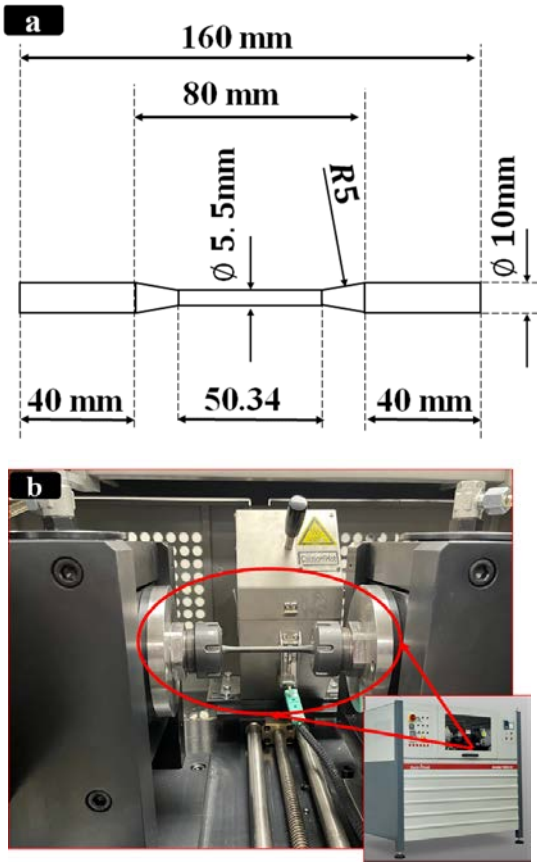


Fig. 1: a) machined specimen geometry and dimensions based on ISO 1143 for RBF test, b) RBF machine and specimen set-up for test.

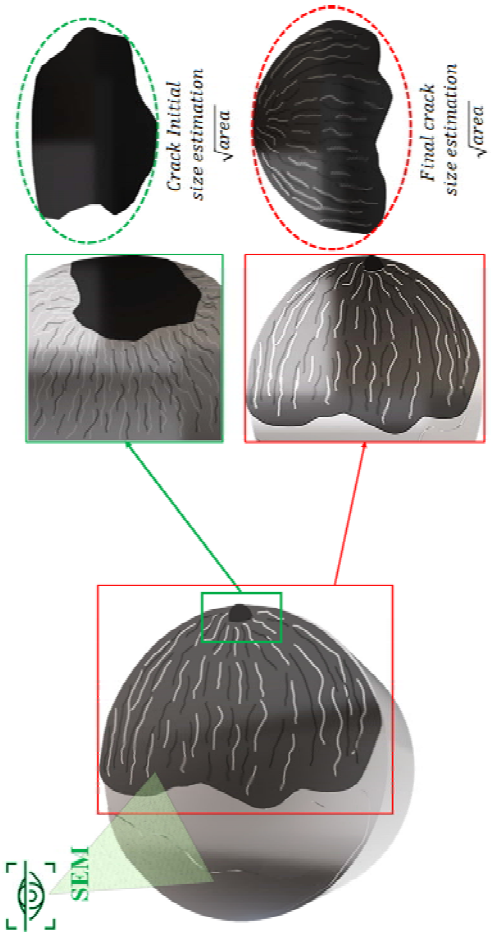


Fig. 2: Fractured surface sectioning and SEM investigation strategy for initial and final crack length estimation by root area method.

3. RESULTS AND DISCUSSION

3.1. Mechanical properties

3.1.1. Tensile Properties

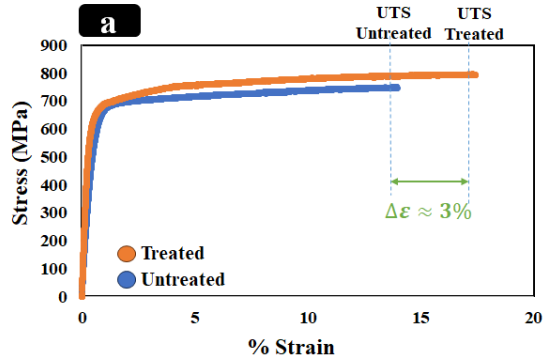
The tensile test results in Fig. 3 indicated that Young's modulus (slop of diagrams in the elastic area) and elongation of the material increased in tandem with the surface treatment. Subsequently, the stress-strain diagram of both the treated and untreated samples is depicted in Fig. 3 (a). It appears that the treated sample exhibited nearly 3% more strain after the diagram during the specified testing period (180 seconds following the commencement of the tensile test). The dash lines in Fig. 3(b) indicate the yield strength of 0.2% offset of both types of materials. The results indicate that the yield strength of the samples was enhanced following the surface treatment. The extensometer was removed after 18% strain during the test. Consequently, the ultimate tensile strength (UTS) was determined using polynomial regression on empirical data from the yield strength point to the end of the 18% strain. The final UTS was estimated with an accuracy of

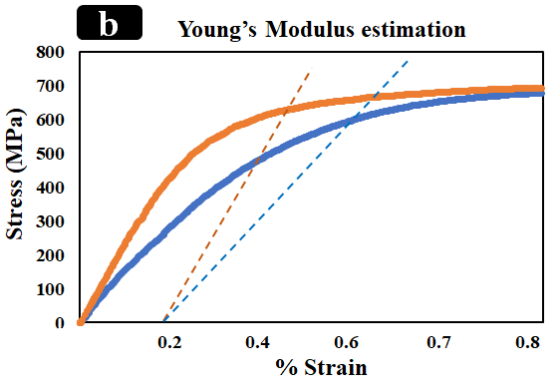
95% for untreated samples and 98% for treated samples using the regression model. Table 2 presents a summary of the tensile parameters of both specimens. The changes in yield strength resulting from surface treatment would have a significant impact on the fatigue properties of this material, especially the surface layer may have a large change in tensile properties rather than the entire material.

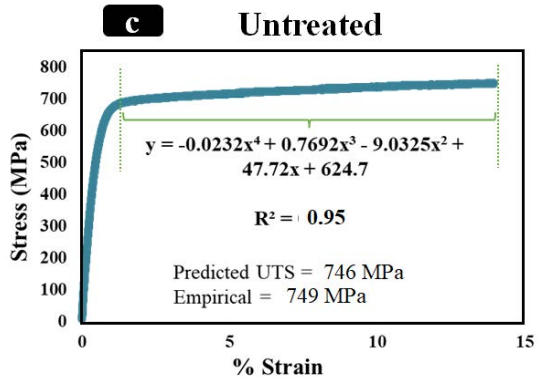
The simultaneous increase in elongation and ultimate tensile strength, as shown in Fig. 3(a) to (d), indicates an overall increase in material toughness (the entire area under the diagrams). Given that this treatment was applied to the surface, any alterations in the characteristics of the surface layer could have a major impact on the fatigue properties under the RBF test. The RBF test revealed that the most stress was experienced on the surface of the specimen, and all cracks originated from the surface layer [5, 6]. Thus, it is anticipated that enhancing the mechanical properties through surface treatment will have a substantial impact on the fatigue properties of this material.

Table 2: Summary of tensile properties of treated and untreated specimens

Specimen	Tested σ_{yield} (MPa)	Tested σ_{UTS} (MPa)	Predicted σ_{UTS} (MPa)
Untreated	627	749	746
Treated	642	795	796







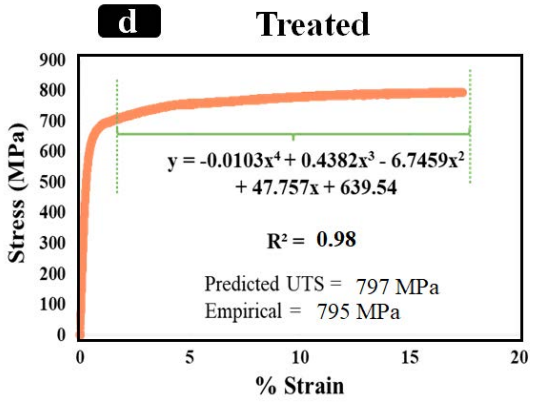


Fig. 3: a) Tensile test data for both treated and untreated specimens, b) Elastic area view, c) and d) Polynomial regression of plastic deformation area and UTS estimation.

3.1.2. Fatigue Properties

Following the surface treatment, the S-N data of the treated specimens demonstrated a significant improvement in fatigue endurance and overall fatigue strength, as evidenced by the increase in yield strength, and technical toughness of the material. It appears that the untreated specimens exhibited a fatigue limit of 405 MPa, as indicated in Fig. 4. This behavior showed a direct relation, as the lifetime increased as the stress level decreased. The treated specimens exhibited a fatigue limit of 545 MPa and a slightly dispersed distribution of data in the high-stress levels, which abruptly dropped to the fatigue limit with a very narrow stress range between 10^4 and 10^7 lifetimes. Consequently, the surface treatment resulted in an approximately 34% increase in the fatigue limit (from 405 to 545 MPa) due to a 2.5% increase in yield strength. This is a significant accomplishment in the enhancement of material durability in engineering design. In this study, a highly significant event was observed: the plastic bending of treated specimens at high-stress levels without any fracture or surface cracking. This observation is the cause of the dispersed data in the higher stress level of the treated specimens' S-N curve, which is a result of the plastic bending of the samples during the RBF test. It is important to mention that although the

fracture did not occur on surface-treated specimens, the practical bending is considered a failure since the material is permanently deformed. Therefore, the failed lifetime is not equal to a fractured lifetime, and probably the fracture may happen in a more extended lifetime (of course if the specimen does not bend).

The tensile properties were enhanced by the surface treatment; however, this enhancement was attributed to changes in the surface layer's properties rather than the interior of the sample. Therefore, the surface layer will not pass the yield strength at higher stress levels; however, the interior of the sample will pass the yield strength (due to its nearly identical properties to the untreated sample). Consequently, the entire sample will be plastically bent, and the RBF test will be terminated. This stop is a failure, but it does not involve any fractures. This is because the material has passed the elastic domain and is not in a state of high cyclic fatigue and plastically deforms. To further explain this phenomenon, the schematic in Fig. 5 illustrates the distribution of stress gradients in the cross-section of the specimen during the RBF test. In Fig. 5(a), it appears that the maximum stress will occur on the surface of the material and will decrease linearly through the neutral axis in the center of the specimen. Consequently, the surface that undergoes the treatment may exhibit distinct mechanical properties compared to the inner layers. Thus, as depicted in Fig. 5(b), when subjected to stress levels higher than the yield strength of the untreated specimen, the inner layer of the specimen may surpass its yield strength and undergo plastic deformation, while the surface stress remains below the yield strength of the treated specimen (the surface will follow the treated yield strength and interior layers will follow close to untreated yield strength).

The relationship between the surface behavior of the surface-treated specimen and the interior layers of the specimen, which have nearly the same mechanical properties as the untreated specimen, is of paramount importance in the infinite life design criteria, which are founded on the fatigue limit. For instance, the interior layer behavior and layer behavior are significant when designing based on the fatigue limit of the treated specimen. The maximal layer thickness of the interior layer can be determined by a rough estimation, as it is under the fatigue limit stress amplitude of 405 MPa. The remaining layer thickness on the surface is under the stress amplitude of 545 MPa, which is equal to the fatigue limit of treated samples. Therefore, the specimen's surface is subjected to this stress level, as the fatigue limit of treated specimens is 545 MPa (purple data in Fig. 4). Conversely, we can assume a linear gradient from the surface to the neutral axis (Fig. 5(a)). Consequently, the stress equation concerning the sample radius will be written as Eq. 1 when using linear estimation:

$$\boldsymbol{\sigma = 242.2\, r} \qquad \textbf{Eq. 1}$$

in which $\boldsymbol{r}$ is the radius of each layer mm, $\boldsymbol{\sigma}$ is the stress at the point of $\boldsymbol{r}$ as MPa.

By substituting the fatigue limit of untreated samples (405 MPa), the maximum radius of the sample that is not subjected to plastic deformation will be 1.67 mm (the total radius of the sample is 2.25 mm). Therefore, referring to Fig. 5(b) the treated sample which is under fatigue limit stress level (545 MPa), will have an interior layer up to 1.67 mm radius which is experiencing fatigue limit of untreated sample's stress level, and the layer between this radius to the surface would exceed to the plastic deformation. Consequently, the green area in Fig. 5(b) will decrease and the blue area will increase as the stress level in the treated specimen S-N curve increases greater than the endurance of the treated specimen. The treatment condition determines the thickness of the orange area (treated layer).

Another crucial factor to consider is the effect of residual stress on the surface layer caused by the surface treatment. After treatment, the surface layer experiences considerable compressive residual stress, which is balanced by tension stress at the substrate's boundary. Tensile stress occurs when the nitrocarburized case experiences high compressive residual stress. Following the superposition of residual stress and applied stress, the area of the subsurface closest to the boundary between the nitrocarburized case and the substrate received the most stress (see Fig. 5(c)), the dashed line of stress distribution) [18, 26]. Furthermore, the elastic-plastic characteristics of the base material and the carburized casing differ significantly at room temperature. This variation in characteristics may cause strain inconsistency along the boundary during fatigue loading. The influence of residual stress on the surface, as well as its effect on resistance to fracture initiation and propagation, is another important factor that should be investigated further.

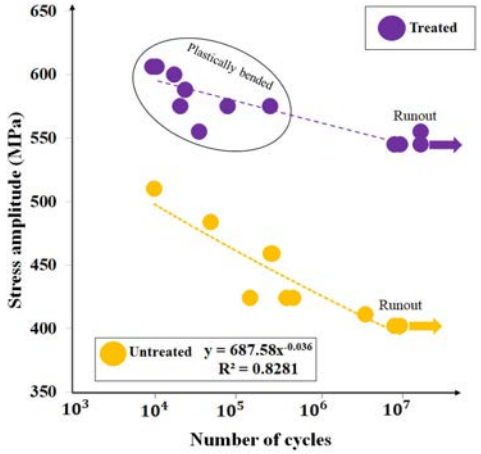


Fig. 4: S-N data of both treated (purple) and untreated (orange) specimens RBF test results with fitted Basquin equation for untreated data.

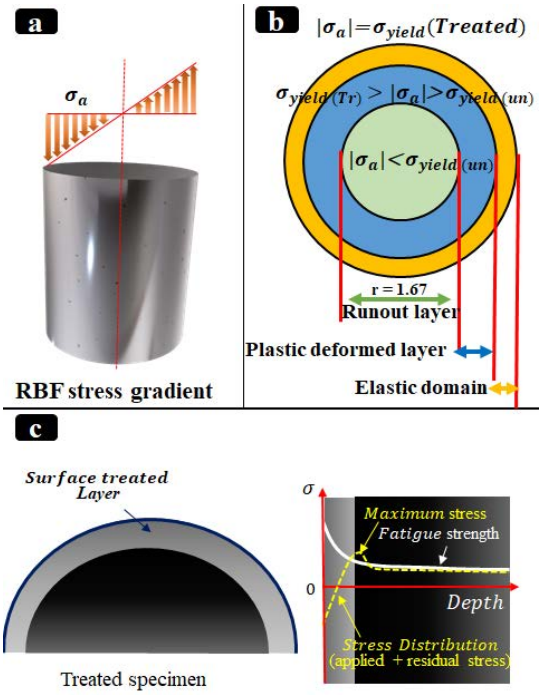


Fig. 5: Schematic illustrating (a) the stress gradient distribution in the cross-section of an RBF sample [6]; (b) the elastic domain of the surface layer, the interior runout layer, and the plastically deformed middle layer; c) stress distribution in the surface layer and the effect of residual stress beneath the surface layer (regenerated from Liu et al [18]).

3.2. Fractography

The fractography investigation was conducted by SEM to further investigate the fatigue properties. However, the treated specimens were never broken, and all the failures were caused by plastic bending. Consequently, due to these reasons, it was not feasible to investigate the fracture surface and the impact of the surface-treated layer on the initiation of the crack. Nevertheless, all of the untreated specimens that failed during RBF tests fractured, and the majority of the SEM images of two distinct stress levels– one near the runout condition and the other near the high-stress levels– are depicted in Fig. 6. It appears that both samples exhibited crack initiation from the surface layer, which was subjected to the highest stress level. It is evident that the white marks on the propagation areas almost converge to a single point on the surface, which is referred to as the crack initiation site. This indicates that there are no multiple stable crack initiation and propagation on these samples. Both specimens exhibited a stable crack propagation area until the final brittle fracture. However, it appears that the area of propagation increased as the stress level in the RBF test decreased from 77% to 67% of the yield strength. By increasing the magnification on the crack initiation site, it becomes apparent that there is a defect present at the initiation point of both samples. This flaw is indicated by yellow dashed lines in Fig. 7. The stress concentration around these defects (inclusions) appears to be the cause of the crack start. Therefore, estimating the magnitude of these defects is necessary for predicting the fatigue lifetime using modeling techniques. In Fig. 7(a), the distance between two flaws is smaller than their respective sizes (distance is 28 μm). Therefore, according to Tajiri et al.'s [27] concept of equal root area, we treat both defects as a single entity and calculate the square root of the sum of their areas. The calculated defect size in Fig. 7(a) is 37.6 μm. The inclusion in Fig. 7(b) has a defect size of 32.8 μm using the same procedure as calculated by Eq. 2.

$$Defect\ size = \sqrt{area} \qquad \textbf{Eq. 2}$$

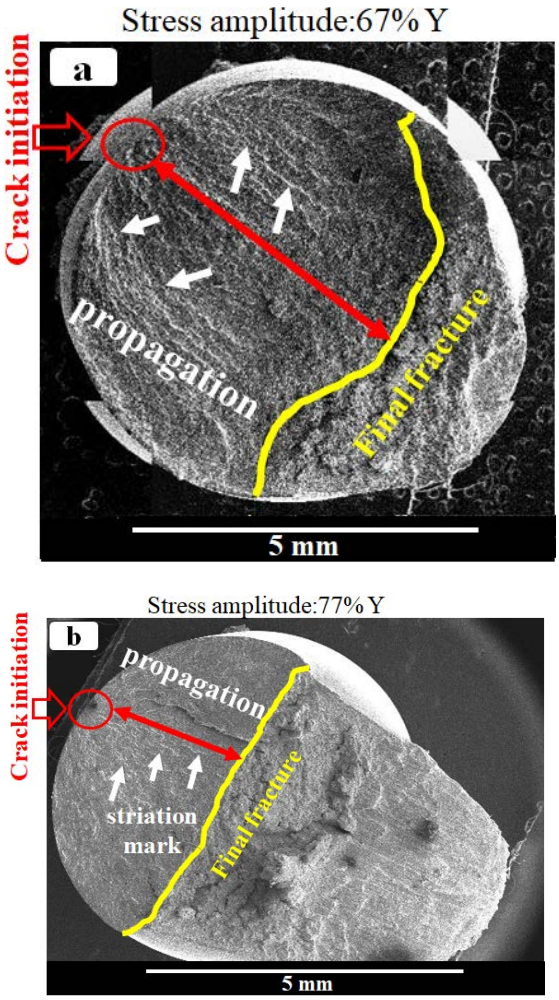


Fig. 6: SEM images of fractured untreated specimens under stress levels of 67% and 77% of yield strength.

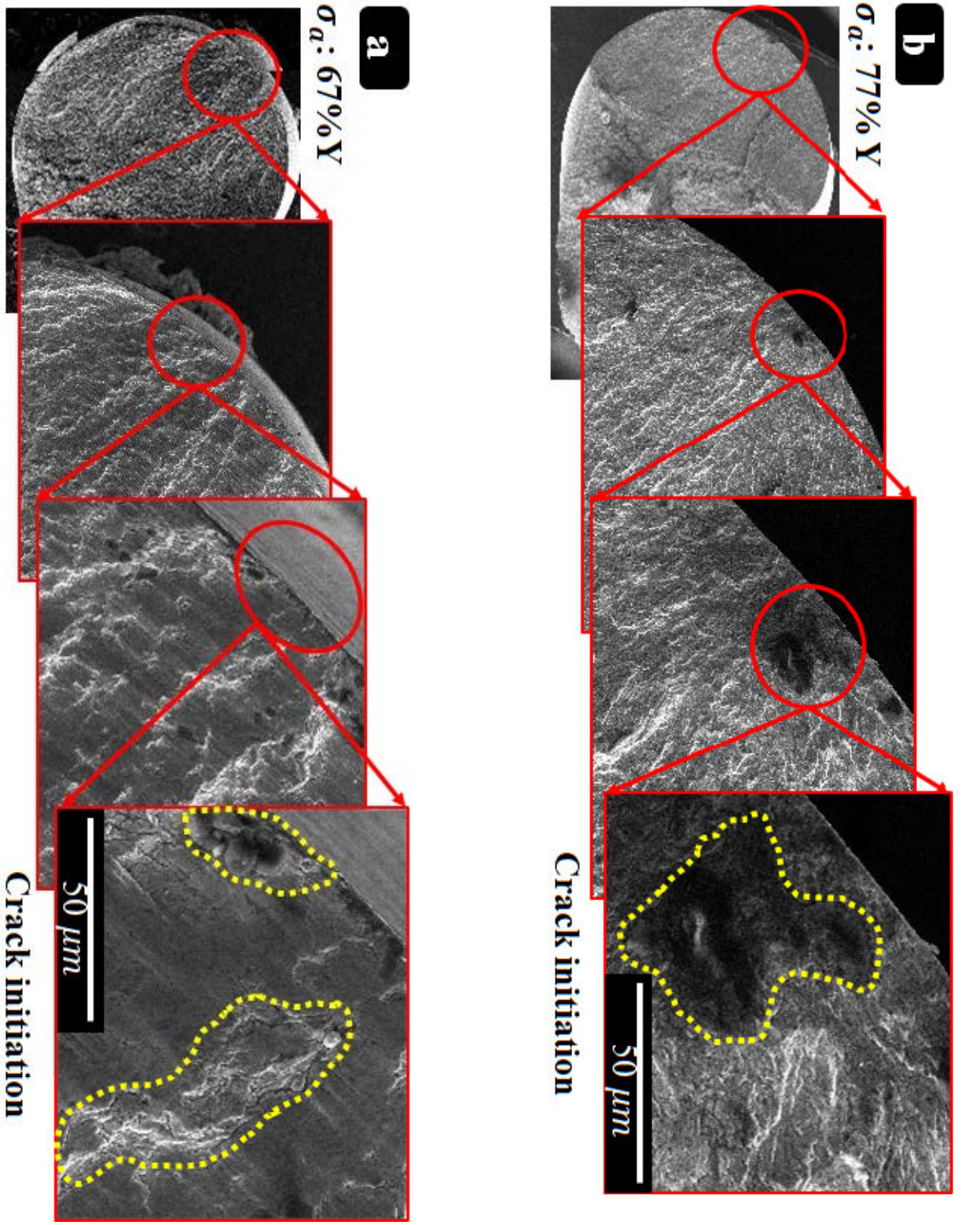


Fig. 7: Higher magnification of SEM images of each specimen crack initiation area, test specimen under a) 67% and b) 77% of yield strength in RBF test.

3.3. Modeling

In the field of linear elastic fracture mechanics (LEFM), the stress intensity factor (SIF) is commonly considered to be the main driving force responsible for the growth of cracks. When the change in Δk, exceeds the threshold value Δk_{th}, the crack is propagating. The extent of crack expansion for lengthy cracks may show a clear association with the SIF using the Paris formula [28, 29]:

$$\frac{da}{dN} = C^*.(\Delta k - \Delta k_{th})^m \qquad \text{Eq. 3}$$

$C^*$and m, are two material parameters equal to 5.026×10^{-10} and 3.531, respectively, according to Shih and Chen's study [30]. On the other hand, the Δk_{th} can be defined based on Murakami's equation in Eq. 4:

$$\Delta k_{th} = g(HV + 120)a^{\frac{2}{n}}(\frac{1-R}{2})^{\alpha} \qquad \text{Eq. 4}$$

where $g = 3.3 \times 10^{-3}$ and 2.77×10^{-3}, for external and internal cracks respectively, HV is the Vickers hardness, $a = \sqrt{area}$ is the crack length (or defect projected length) in μm, R is the stress ratio, n is an exponent in the original Murakami's model and $\alpha = 0.226 + HV \times 10^{-4}$. Therefore, assuming the initial crack length equal to the defect size and the final crack length equal to the root area of the propagation domain (based on Fig. 8 (a) and (b) estimation), Eq. 4 can be combined with Eq. 3 and generate Eq. 5:

$$\frac{da}{dN} = C^*.(g(HV + 120))^m.(a^{2/n} - a_{in}^{2/n})^m \qquad \text{Eq. 5}$$

With substituting the HV= 184.5 for this material, the final equation for estimating N_f will be:

$$N_f = \int_{a_{in}}^{a_f} \frac{1.956\times10^9}{(a^{\frac{1}{3}} - a_{in}^{\frac{1}{3}})^{3.531}}.da \qquad \text{Eq. 6}$$

The prediction accuracy of this equation is less than 50%, which means the model is not completely consistent due to very limited data (just two fractured surface measurements). Therefore, it is not possible to adjust the model empirical coefficients accurately, although this model worked properly for SS316 [31], does not perform for this SS304. Therefore, it is necessary to use the statistical data of the S-N curve in Fig. 4 to develop an accurate model. In this regard, Machine Learning (ML) techniques have been utilized for analyzing the statistical data of the RBF test to model the cycle on numbers (lifetime) according to stress amplitude, RPM, and condition of specimens (treated or untreated).

3.3.1. Machine Learning (ML)

Machine learning has been employed to conduct the statistical modeling section. Deep learning techniques were not feasible due to the dataset's small size, and the limited features necessitated the use of machine learning. The random forest regression (RFR) model was chosen as the most effective model after several machine learning methods were applied to the data. The stress amplitude, RPM, and surface treatment condition are the features that have been chosen for ML in this study. The response is significantly influenced by the stress magnitude factor, which is the primary feature and primary factor in the S-N diagram. RPM, which is a representative of frequency, has been incorporated into this study due to its substantial impact on the test as a result of self-heating phenomena. The surface treatment factor has been defined as a categorical factor, with two levels: zero for untreated specimens and one for treated specimens.

The model was trained on 80% of the data (17 data), with the remaining 20% (5 data) used for testing. The data set selection for the test was made in a broad range, from high-stress levels to runout steel levels, and the middle of the data set to ensure uniform testing of the model. The feature importance determination was completed after further testing of the model and comprehending the significance of each parameter on the fatigue test. The feature importance reflects each variable's contribution to the model's predictive performance by quantifying how much each feature reduces the impurity in the decision trees. Impurity reduction is measured by the variance reduction at each node split in the case of regression. For each split in the forest, the selected feature decreases the variance (mean squared error) of the target variable, and the amount of this reduction is accumulated for that feature across all trees. The accumulated reductions are normalized to provide a relatively important score between 0 and 1 for each feature. The outcome of the feature importance study (Fig. 9(a)) indicated that stress level is the most critical factor, followed by RPM, which is associated with self-heating phenomena, and treatment.

The model's performance was evaluated using the Root Mean Square Error (RMSE), which quantifies the difference between the predicted and actual cycle values. The RMSE for the test set was approximately 1,173,137 cycles, which indicates the average error in the predictions. The RFR model yielded highly accurate predictions compared to the experimental data, as demonstrated in Fig. 8(c) with an R^2 value of 86.8% which was higher than LEFM classical model accuracy, even more than Basquin equations (Fig. 4). Although the model is exhibiting rather decent accuracy in its predictions, the restricted size of the dataset is still negatively impacting the reliability and accuracy of the model. The RFR model utilizes decision trees and does not produce any prediction mathematical equation, therefore it is not possible to calibrate the model with experimental correction coefficients. However, this trained model, based on the database, effectively predicts the lifetime of SS304 under RBF test under two surface conditions: treated and untreated with high accuracy as shown in Fig. 8(c).

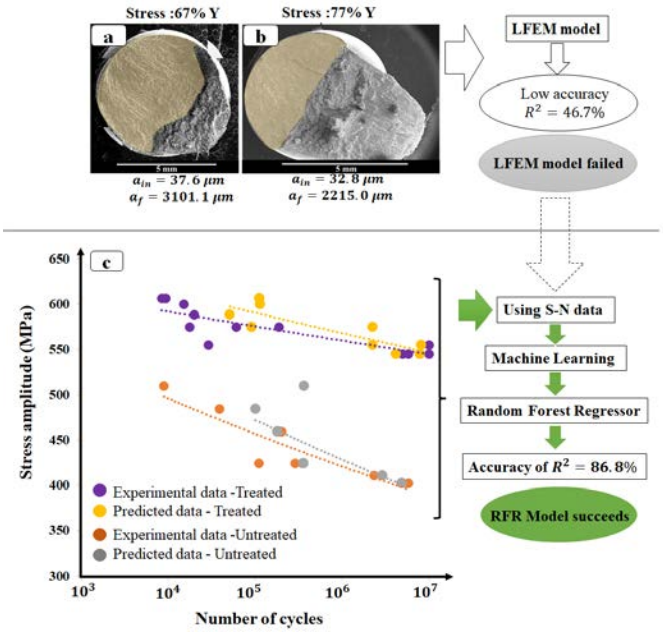


Fig. 8: a &b) demonstration of calculated initial and final length based on the root area, c) experimental and predicted data by RFR model, and the logic of choosing the best model with higher accuracy.

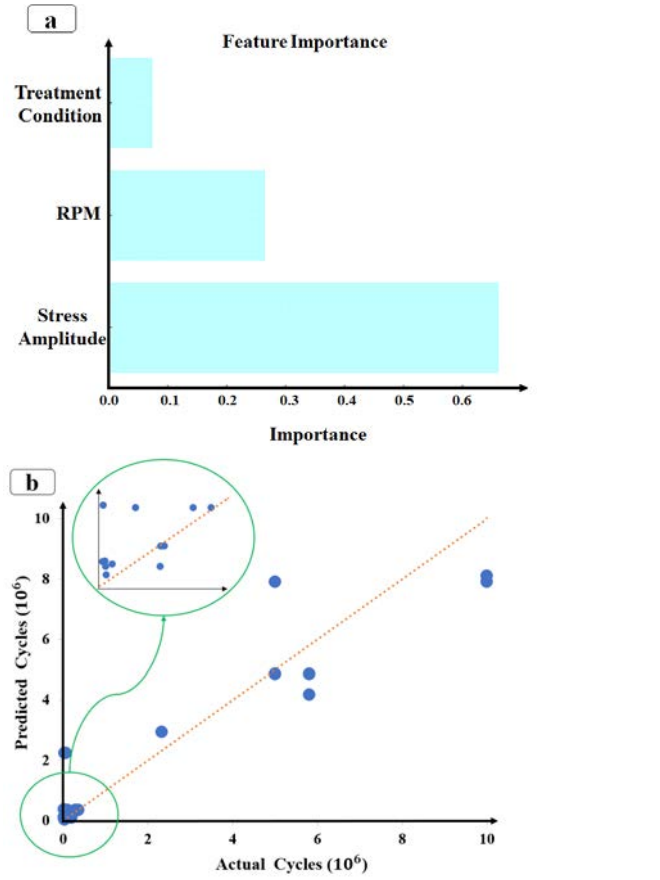


Fig. 9: a) Feature importance diagram of modeling factors effect on the response, b) the predicted vs actual data diagram.

4. SUMMARY

This study conducted a comprehensive analysis of the fatigue durability of wrought SS304 under RBF circumstances, specifically comparing the performance of specimens that had surface treatment with those that did not. The experimental findings demonstrated that surface treatment had a substantial impact on fatigue resistance, as indicated by a notable rise in fatigue limit from 405 MPa for untreated samples to 545 MPa for treated samples (34% enhancement). The improvement can be credited to the surface treatment, which probably created a layer of compressive residual stress on the surface [32, 33], in addition, the diffused NFC environment atoms through the surface layer may compacted the slip plane regions and made dislocation movements difficult [34, 35]. NFC induces compressive residual stresses and impedes dislocation movement by counteracting external tensile stress, the compressive residual stress layer, which is the result of atom diffusion into the surface, enhances fatigue strength by preventing crack initiation and propagation. Furthermore, the crystal lattice is distorted by the diffused atoms (carbon or nitrogen), which restricts dislocation mobility and compacts slip planes[36, 37]. This layer enhances the material's ability to withstand the start and spread of cracks when subjected to repeated loading. The specimens that were not treated showed a fatigue endurance of 405 MPa, which is equivalent to 65% of their yield strength, after undergoing 5 million cycles. On the other hand, the specimens that underwent surface treatment exhibited an endurance of 545 MPa, which corresponds to 85% of their yield strength.

An important observation was that the failure mode in treated specimens (in this study) changed from the typical fracture to plastic bending when subjected to greater stress levels. Untreated specimens usually experience failure due to the initiation and propagation of cracks on the surface. In contrast, treated specimens showed no signs of surface cracks, even under greater stress conditions. However, the failures were caused by plastic deformation occurring in the inner layers, whereas the outer layer remained within the elastic range. The phenomena can be attributed to the variation in stress levels across the cross-section of the specimen. The outside layer, which was treated, remained intact even under high levels of stress, while the inside, which had qualities comparable to the untreated material, underwent plastic deformation. The Basquin equation, commonly employed for fatigue life estimation, was discovered to be inadequate in considering the impacts of surface treatment since the treated specimens did not show any fracture failure. On the other hand, an experimental dataset was used to construct an ML model, especially an RFR. The RFR model accurately predicted the fatigue life, achieving a high R^2 value of 86.8%, which was much better than standard models. The model demonstrated an RMSE of around 1,173,137 cycles, demonstrating a strong predicted accuracy despite the small dataset.

The use of surface treatment not only increased the fatigue limit by 34% but also changed how failure occurs, transitioning from fatigue caused by cracks to plastic deformation of the material. Utilizing ML for fatigue life prediction demonstrated efficacy, providing a superior and dependable technique compared to traditional methods. These findings offer useful knowledge for the development and production of SS304 components that can withstand fatigue, particularly in situations with high levels of stress. Subsequent investigations should prioritize the enlargement of the dataset for ML models and the examination of the enduring consequences of surface treatments in different operational circumstances.

REFERENCES

[1] R.R. Kumar, R.K. Gupta, A. Sarkar, M. Prasad, Vacuum diffusion bonding of α-titanium alloy to stainless steel for aerospace applications: Interfacial microstructure and mechanical characteristics, Materials Characterization 183 (2022) 111607.

https://doi.org/10.1016/j.matchar.2021.111607

[2] K.K. Pradhan, C.R. Matawale, Heat treatment analysis of SS304 for gas turbine application, Materials Today: Proceedings 33 (2020) 5734-5739.

https://doi.org/10.1016/j.matpr.2020.05.102

[3] A. Arifin, I. Yani, Failure analysis of AISI 304 stainless steel pipeline transmission a petrochemical plant, IOP Publishing, p. 012006.

https://doi.org/10.1088/1757-899X/857/1/012006

[4] H.M. Raheem, I. Altayer, H.S. Mohamed, M.H. Al-maamori, Metallurgical Failure Analysis: A Case Study of Observing a Leak in a Stainless Steel SS304 Pipe, Petroleum Chemistry 64(1) (2024) 134-143.

https://doi.org/10.1134/S096554412402004X

[5] A. Behvar, Y. Aghayar, M. Avateffazeli, A. Tridello, A. Benelli, D.S. Paolino, M. Mohammadi, M. Haghshenas, Synergistic impact of corrosion pitting on the rotating bending fatigue of additively manufactured 316L stainless steel: Integrated experimental and modeling analyses, International Journal of Fatigue 188 (2024) 108491.

https://doi.org/10.1016/j.ijfatigue.2024.108491

[6] A. Behvar, F. Berto, M. Haghshenas, A review on isothermal rotating bending fatigue failure: Microstructural and lifetime modeling of wrought and additive manufactured alloys, Fatigue & Fracture of Engineering Materials & Structures 46(10) (2023) 3545-3595.

https://doi.org/10.1111/ffe.14094

[7] K.S. Chan, Roles of microstructure in fatigue crack initiation, International Journal of Fatigue 32(9) (2010) 1428-1447.

https://doi.org/10.1016/j.ijfatigue.2009.10.005

[8] T. Mura, A theory of fatigue crack initiation, Materials Science and Engineering: A 176(1-2) (1994) 61-70.

https://doi.org/10.1016/0921-5093(94)90959-8

[9] R.I. Stephens, A. Fatemi, R.R. Stephens, H.O. Fuchs, Metal fatigue in engineering, John Wiley & Sons2000.

Link: Book

[10] S. Yang, W. Zeng, J. Yang, Characterization of shot peening properties and modelling on the fatigue performance of 304 austenitic stainless steel, International Journal of Fatigue 137 (2020) 105621.

https://doi.org/10.1016/j.ijfatigue.2020.105621

[11] S. Yang, Investigations on the changed intensity shot peening specimens machined from SS304: process characterization, fatigue modeling, and failure analyses, The International Journal of Advanced Manufacturing Technology 120(7) (2022) 5041-5056.

https://doi.org/10.1007/s00170-022-09063-w

[12] B.B. Fernandes, S. Mändl, R.M. Oliveira, M. Ueda, Mechanical properties of nitrogen-rich surface layers on SS304 treated by plasma immersion ion implantation, Applied Surface Science 310 (2014) 278-283.

https://doi.org/10.1016/j.apsusc.2014.04.142

[13] C. Ye, C. Zhang, J. Zhao, Y. Dong, Effects of post-processing on the surface finish, porosity, residual stresses, and fatigue performance of additive manufactured metals: a review, Journal of Materials Engineering and Performance 30 (2021) 6407-6425.

https://doi.org/10.1007/s11665-021-06021-7

[14] L. Shen, L. Wang, Y. Wang, C. Wang, Plasma nitriding of AISI 304 austenitic stainless steel with pre-shot peening, Surface and Coatings Technology 204(20) (2010) 3222-3227.

https://doi.org/10.1016/j.surfcoat.2010.03.018

[15] Y.-H. Chung, T.-C. Chen, H.-B. Lee, L.-W. Tsay, Effect of micro-shot peening on the fatigue performance of AISI 304 stainless steel, Metals 11(9) (2021) 1408.

https://doi.org/10.3390/met11091408

[16] K. Praveenkumar, S. Swaroop, G. Manivasagam, Effect of multiple laser peening on microstructural, fatigue and fretting-wear behaviour of austenitic stainless steel, Surface and coatings technology 443 (2022) 128611.

https://doi.org/10.1016/j.surfcoat.2022.128611

[17] J. Colin, A. Fatemi, S. Taheri, Fatigue behavior of stainless steel 304L including strain hardening, prestraining, and mean stress effects, (2010).

https://doi.org/10.1115/1.4000224

[18] Z. Liu, S. Wang, Y. Feng, X. Wang, Y. Peng, J. Gong, Exploration on the fatigue behavior of low-temperature carburized 316L austenitic stainless steel at elevated temperature, Materials Science and Engineering: A 850 (2022) 143562.

https://doi.org/10.1016/j.msea.2022.143562

[19] S. Aguado-Montero, J. Vázquez, C. Navarro, J. Domínguez, Optimal shot peening residual stress profile for fatigue, Theoretical and Applied Fracture Mechanics 116 (2021) 103109.

https://doi.org/10.1016/j.tafmec.2021.103109

[20] T. Wiriyasaroj, P. Juijerm, B. Scholtes, T. Niendorf, Fatigue and cyclic deformation behavior of non-and boronized austenitic stainless steel AISI 304 at room and elevated temperatures, Songklanakarin Journal of Science & Technology 41(2) (2019).

https://www.thaiscience.info/Journals/Article/SONG/10993250.pdf

[21] D. Kumar, S. Idapalapati, W. Wang, S. Narasimalu, Effect of surface mechanical treatments on the microstructure-property-performance of engineering alloys, Materials 12(16) (2019) 2503.

https://doi.org/10.3390/ma12162503

[22] I. Altenberger, B. Scholtes, Improvement of fatigue behaviour of mechanically surface treated materials by annealing, Scripta materialia 41(8) (1999) 873-881.

https://doi.org/10.1016/S1359-6462(99)00222-5

[23] S. Suresh, Graded materials for resistance to contact deformation and damage, Science 292(5526) (2001) 2447-2451.

https://doi.org/10.1126/science.1059716

[24] S.M. Banavasi, K.S. Ravishankar, S.N. Padmayya, A Review on Design and Fabrication of Fatigue Testing Machine, International Journal of Novel Research and Development 3(5) (2018) 5-14.

ISSN: 2456-4184

[25] J.M.E. Marques, D. Benasciutti, A. Niesłony, J. Slavič, An overview of fatigue testing systems for metals under uniaxial and multiaxial random loadings, Metals 11(3) (2021) 447.

https://doi.org/10.3390/met11030447

[26] Z. Liu, S. Wang, Y. Feng, Y. Peng, J. Gong, M.A.J. Somers, Residual stress relaxation in the carburized case of austenitic stainless steel under alternating loading, International Journal of Fatigue 159 (2022) 106837.

https://doi.org/10.1016/j.ijfatigue.2022.106837

[27] A. Tajiri, T. Nozaki, Y. Uematsu, T. Kakiuchi, M. Nakajima, Y. Nakamura, H. Tanaka, Fatigue limit prediction of large scale cast aluminum alloy A356, Procedia materials science 3 (2014) 924-929.

https://doi.org/10.1016/j.mspro.2014.06.150

[28] C.A. Molina, M.D. Chapetti, Estimation of high cycle fatigue behaviour using a threshold curve concept, International Journal of Fatigue 108 (2018) 47-52.

https://doi.org/10.1016/j.ijfatigue.2017.11.007

[29] W.W. Gerberich, S.E. Harvey, D.E. Kramer, J.W. Hoehn, Low and high cycle fatigue—A continuum supported by AFM observations, Acta materialia 46(14) (1998) 5007-5021.

https://doi.org/10.1016/S1359-6454(98)00169-4

[30] Y.-S. Shih, J.-J. Chen, The frequency effect on the fatigue crack growth rate of 304 stainless steel, Nuclear engineering and design 191(2) (1999) 225-230.

https://doi.org/10.1016/S0029-5493(99)00144-2

[31] A. Behvar, Y. Aghayar, M. Avateffazeli, A. Tridello, A. Benelli, D.S. Paolino, M. Mohammadi, M. Haghshenas, Synergistic impact of corrosion pitting on the rotating bending fatigue of additively manufactured 316L stainless steel: Integrated experimental and modeling analyses, International Journal of Fatigue (2024) 108491.

https://doi.org/10.1016/j.ijfatigue.2024.108491

[32] E. Macherauch, Introduction to residual stress, Advances in surface treatments 4 (2014) 1-36.

Link: Book

[33] H. Arora, R. Singh, G.S. Brar, Numerical simulation on residual stresses of stainless steel SS-304 thin welded pipe, Measurement and Control 53(7-8) (2020) 1183-1193.

https://doi.org/10.1177/0020294020917173

[34] D.J. Bacon, Y.N. Osetsky, D. Rodney, Dislocation–obstacle interactions at the atomic level, Dislocations in solids 15 (2009) 1-90.

https://doi.org/10.1016/S1572-4859(09)01501-0

[35] I. Baker, Interstitial strengthening in fcc metals and alloys, Advanced Powder Materials 1(4) (2022) 100034.

https://doi.org/10.1016/j.apmate.2022.100034

[36] B. Clausen, M. Steinbacher, F. Hoffmann, Residual Stresses and Distortion in Thermochemically Treated Steels, Steel Heat Treating Technologies, ASM International2014, pp. 375-390.

https://doi.org/10.31399/asm.hb.v04b.a0005956

[37] S. Jegou, L. Barrallier, R. Kubler, Residual stress development during nitriding of steels, Trans Tech Publ, pp. 370-373.

https://doi.org/10.4028/www.scientific.net/MSF.681.370